An Approach for the Detection of Proliferative Diabetic Retinopathy

J.Sweetline Arputham
PG Student,Dept of CSE
Government College of Engineering, Tirunelveli.

G.Tamilpavai
Asst.Prof., Dept of CSE
Government College of Engineering, Tirunelveli.

S.Tamilselvi
Asso.Prof., Dept of ECE
National Engineering College
Kovilpatti.

ABSTRACT
Proliferative diabetic retinopathy is the most advanced stage of diabetic retinopathy, and is classified by the growth of new blood vessels. These blood vessels are abnormal and fragile, and are susceptible to leaking blood and fluid onto the retina, which can cause severe vision loss. This paper proposes a method by combining prior works of Keith A.Goatman et al.(2011) and Gopal Datt Joshi et al (2011) for the detection of proliferative diabetic retinopathy. First, vessel-like patterns are segmented by using Ridge Strength Measurement and Watershed lines. The second step is measuring the vessel pattern obtained. Many features that are extracted from the blood vessels such as shape, position, orientation, brightness, contrast and line density have been used to quantitate patterns in retinal vasculature. Based on the features extracted, the segment is classified as normal or abnormal by using Support Vector Machine Classifier. The obtained accuracy may be sufficient to reduce the workload of an ophthalmologist and to prioritize the patient grading queues.

Keywords
Diabetic Retinopathy, Microaneurysm, Vasculature, Watershed Transformation, Optic Disc.

1. INTRODUCTION
Diabetic Retinopathy (DR) is a severe and widely spread eye disease characterised by abnormal high blood sugar (hyperglycaemia) resulting from low levels of the hormone insulin. The progression of retinopathy is from mild non-proliferative abnormalities such as microaneurysm, to moderate and severe non-proliferative abnormalities such as exudates and haemorrhages, to proliferative diabetic retinopathy characterised by the abnormal vessel changes such as venous beading, intra-retinal microvascular abnormalities (IRMA) and growth of new blood vessels. Without timely treatment, the new blood vessels can bleed, leading to vitreous haemorrhage, fibrosis and retinal detachment.

New blood vessels have a narrower calibre, more tortuous and are convoluted than normal vessels. New blood vessels are classified based on the position as new vessels on the optic disc and new vessels elsewhere. The development of the new vessels can be inhibited by early diagnosis and treatment. Hence, screening of all diabetic patients (even without vision impairment) would help to diagnose the disease early enough for an optimal treatment. Although the prevalence of proliferative diabetic retinopathy is low, the onset of vision loss is considerably high.

A number of studies have been made regarding the detection of microaneurysm [2], which is the first sign of diabetic retinopathy. The work of J.H.Hipwel *et al* was based on the algorithm that enhances the round features and classify it as microaneurysms based on the intensity and size of the features[3] T.Walter *et al* detect microaneurysm by using the diameter closing and an automatic threshold scheme[4]. Some investigations has been made for detecting haemorrhages and exudates[5]-[9]. T.Walter *et al* uses the high grey level variation for detecting exudates [10]. A very few work have been made on the detection of the abnormalities of the vessels such as venous beading [11] C.W.Yang et al proposes a method that uses neural network-based shape cognitron to detect venous beading [12].

In this paper we proposed the method by combining the prior works of Optic Disc Segmentation and detection of new vessels to detect the disease Proliferative Diabetic Retinopathy [13] [14]. Since the optic disc is the entry point of most of the blood vessels, we focussed our attention towards the optic disc.

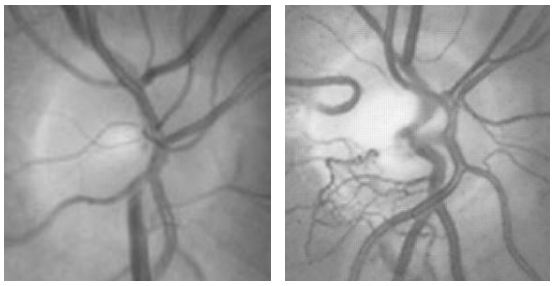

(a) (b)

Fig 1(a) normal optic disc. (b) optic disc containing abnormal vessels.

2. METHOD
2.1. Preprocessing
The green color plane was used in the analysis since it shows the highest contrast between the vessels and the retina. The green plane image is used for detecting the abnormalities in the vessels. The image was resized and the optic disc is located appropriately [15] [16].

2.1.1 Optic Disc Segmentation
The optic disc can be identified as a bright region on a retinal fundus image. In order to reduce computational time, the approximate locations of optic discs were identified, and regions of interest (ROIs) that included the optic discs were extracted from the images. The red color plane was used in the Optic Disc detection since it gives a better contrast of the OD region. Gopal Datt Joshi et al [17] proposes a multi-dimensional image representation for the segmentation of the disc region. First, Gaussian filter is applied to the image at

three different scales and summed. Second, a special case of texture filter bank is used,

$$L(c,\sigma,\tau) = Lo(\sigma,\tau) = \cos\left(\frac{\pi\tau c}{\sigma}\right)e^{-\frac{c^2}{2\sigma 2}} \qquad (1)$$

where τ represents the number of cycles of the harmonic function within the Gaussian envelope. Next, Gabor filter is used at three different values and the result are summed. Combining all the three steps a resultant image is obtained in which the circular hough transform is applied to initialize the contour. A region-based active contour model which uses local image information at a support domain around each point of interest (POI) inspired by localized C-V models by using a richer form of local image information gathered over a multi-dimensional feature space is used for the segmentation of the optic disc.

2.2. Segmentation of blood vessels

Segmentation of the blood vessels are essential since the abnormal vessels are smaller, more tortuous and convoluted than the normal blood vessels. Several methods have been used for segmentation of the blood vessels [18] [19] [20].

Ridges are defined as points where the image has an extrema in the direction of the largest surface curvature. The ridge strength can be calculated by the dark ridges that is formed by the vessel center lines. Ridge strength k, is given by [21]

$$k = \frac{L^2_x L_{yy} + L^2_y L_{xx} - 2L_x L_y L_{xy}}{(L^2_x + L^2_y)^{3/2}} \qquad (2)$$

where, L represents the Gaussian filtered image, L_x and L_y represents the first partial derivative of L with respect to x and y and L_{xx}, L_{yy}, L_{xy}, L_{yx} represents the second partial derivative of L_x and L_y. The value of the ridge strength **k** is positive for the vessel ridges, negative for areas between the vessels and undefined for the areas where the gradient in both x and y direction is zero

Applying an empirically derived threshold, k_{thres} is used for the segmentation of the blood vessels. The above method produces a large number of disjoint vessels.

Watershed Transformation is the morphological region based segmentation method based on the topology of the image [22][23]. The grey image forms the topographic surface. Watershed Transformation divides the image into regions based on the image grey level. The dividing lines are called the Watershed lines and the grouped regions are called the catchment basins. The grey level is inverted such that the blood vessels form the watershed lines. The inverted grey image is filtered with the Gaussian filter such that over-segmentation can be avoided. The watershed regions are calculated using Meyer's algorithm as

1. A set of markers, pixels where the flooding shall start, are chosen.
2. The neighboring pixels of each marked area are inserted into a priority queue with a priority level corresponding to the grey level of the pixel.
3. The pixel with the highest priority level is extracted from the priority queue. If the neighbors of the extracted pixel that have already been labeled all have the same label, then the pixel is labeled with their label. All non-marked neighbors that are not yet in the priority queue are put into the priority queue.
4. Redo step 3 until the priority queue is empty.

The Watershed Transformation produces closed regions connected by the watershed lines. To remove the non vessel segments the mean value of along each candidate segment is calculated and candidates with mean values less than k_{thres} are discarded.

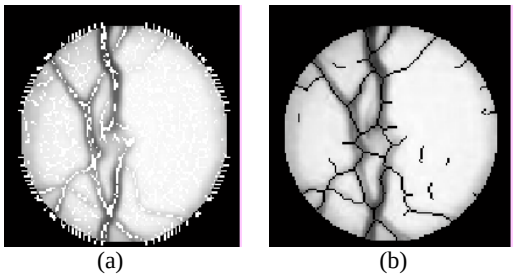

(a) (b)

Fig 2 Blood vessel Segmentation (a) Ridge strength Measurement. (b) Watershed Transformation combines with Ridge strength.

2.3. Feature Measurement

Fifteen features were calculated for each segment, based on characteristics human observers use to recognize abnormal vessels. The vessel origin was estimated as follows. First, a median filter was applied to remove smaller vessels. Next a threshold was applied to select the darkest 20% of pixels, which were assumed to belong to the major blood vessels. The centroid of the result was taken as the approximate origin of the major vessels. The following features were calculated for each segment [24]

1) **Segment length:** The length of each blood vessel from the origin calculated in pixel.

2) **Gradient:** The gradient magnitude of the image at each point gives the direction of the largest possible change in the intensity of the grey image. The gradient is calculated using Sobel gradient operator as

$$G=\sqrt{G_x^2 + G_y^2}. \qquad (3)$$

where G_x ,G_y represents the convolution of original image with the kernel. The mean of the gradient is calculated.

3) **Gradient Variation:** The standard deviation of the Sobel gradient is calculated. This feature is based on the observation that the abnormal vessels have more contrast variation than the normal vessels.

4) **Direction:** The angle between a tangent to the segment center point and a line from its center point to the vessel origin. The feature is based on the observation that normal vessels tend to radiate from the vessel origin towards the edge of the disc, whereas the direction of new vessels is more random.

5) **Tortuosity Measure 1:** The sum of the absolute changes in the tangential direction along segment path

$$T_1 = \frac{1}{n-1}\sum_{i=1}^{n-1} \theta_{i+1} - \theta_i \qquad (4)$$

where, $\boldsymbol{\theta}_i$ is the tangential angle at the *i*th element.

6) **Tortuosity Measure 2:** The difference in the angular extrema of the segment tangents

$$T_2 = \max_{i=1\ldots n}\{\theta_i\} - \min_{i=1\ldots n}\{\boldsymbol{\theta}_i\} \qquad (5)$$

7) **Tortuosity Measure 3:** The third tortuosity measure was the mean change in direction per pixel along the segment.

$$T_3 = \frac{1}{n}\sum_{i=1}^{n} k_i \qquad (6)$$

where,

$$k_i=\begin{cases} 1\ , \ if \begin{cases} \frac{d^2x}{di^2}(i) = 1 \ and \ \frac{d^2y}{di^2}(i) = 0 \\ \frac{d^2x}{di^2}(i) = 0 \ and \ \frac{d^2y}{di^2}(i) = 1 \end{cases} \\ \sqrt{2}, \ if \ \frac{d^2x}{di^2}(i) = 1 \ and \ \left|\frac{d^2y}{di^2}(i)\right| = 1 \\ 0\ , \qquad otherwise \end{cases} \qquad (7)$$

and x and y are the Cartesian coordinates.

8) **Grey Level:** The normalized mean grey level

$$g_{norm} = \frac{1}{G_{max}-G_{min}}\left[\left(\frac{1}{n}\sum_{i-1}^{n} g_i\right) - G_{min}\right] \qquad (8)$$

where g_i is the grey level of the ith segment pixel and G_{max} and G_{min} are the maximum and minimum grey level values in the original image

9) **Grey Level Coefficient of variation:** The ratio of the mean and standard deviation of the segment grey level values.

10) **Distance from origin:** The distance from the center of the segment to the vessel origin in pixel. This feature is based on the observation that the abnormal vessels occur towards the edge of the disc.

11) **Vessel Density:** The segment surrounding the segment 'a' were determined using

$$O(a)=\{b|s(a) \oplus D) \cap s(b) \neq \emptyset$$

where (9)

$$b \in S \text{ and } b \neq a$$

where S is the set of all segments and $s(a) \oplus D$ denotes the dilation between the path of segment 'a' and structuring element D.

12) **Number of Segments:** The total number of segments following the candidate segmentation. This feature is based on the idea that abnormal vessels have more number of segments than normal vessels.

13) **Mean Ridge Strength:**The mean strength of the ridge given by k by the equation (2).

14) **Mean Vessel width:** The distance from each segment point to the closest edge point is assumed to be the vessel half-width at that point.

15) **Mean Vessel wall gradient:** The mean value of the Sobel gradient magnitude for all the vessel wall points.

2.4. Classification

The Support Vector Machine (SVM) [25][26][27] was chosen and used as the classifier for its rapid training and testing phase and for its good classification performance. Support Vector Machine is primarily a linear classifier method that performs classification tasks by constructing hyperplanes in a multidimensional space that separates cases of different class labels. In our paper, it represents two classes such as normal class and abnormal class. The data for a two class learning problem consists of objects labelled with one of two labels corresponding to the two classes; the labels are +1 or -1. Since all the training datas does not exactly lie on the hyperplanes, SVM introduce the notion of a "kernel induced feature space" which casts the data into a higher dimensional space. Although, the kernel finds the linear hyperplane in the transformed space, it looks to be nonlinear in the original feature space. Many kernel mapping functions can be used. But a few kernel functions have been found to work well in for a wide variety of applications. The default and recommended kernel function is the Radial Basis Function (RBF). The kernel function used here was a radial basis function, called the Gaussian kernel, given by

$$K(x_i,x_j)=\exp(-\gamma\|x_i-x_j\|^2) \quad \gamma>0 \qquad (10)$$

where x_i and x_j are the feature vectors for the two classes and γ is a configurable parameter. The degree of the polynomial kernel and the width parameter of the Gaussian kernel control the flexibility of the resulting classifier. All the features were normalized before classification using

$$\hat{a}= \frac{a-m}{s} \qquad (11)$$

where, a is the feature value to normalize and â is the normalized value . m and s are the mean and standard deviation for this feature. They are calculated from the features used to train the classifier so that all the training features have zero mean and unit variance.

2.5. Detector Training and Testing

The system was trained with the normal and abnormal images. As there were too few images with new vessels for separate training and test sets, the SVM was trained and tested simultaneously by leave-one-out cross-validation. The SVM was trained using all the images in the test set except the single test image, and this process was repeated for each image. The feature value normalization was also recalculated each time, leaving out the test image.

3. RESULT

Fig 3 (a) shows the abnormal optic disc (b) the result of the system that classify the vessel segments as abnormal. Fig 4 shows the features corresponding to normal and abnormal images. Fig 5 shows the optic disc that is classified as abnormal.

The sensitivity and specificity are calculated based on the blood vessels classified as normal and abnormal with reference to the manual annotation. Based upon the features considered, it shows different sensitivity and specificity. While considering only the first five features, the system shows the sensitivity and specificity of 66.67% and 76.92% and while considering the first ten features, it shows 83.52% and 84.61% and while taking all the fifteen features, the system achieves sensitivity of 84.7% and specificity of 86.1%.This is plotted in the graph in Fig 6.The obtained accuracy can be sufficient to reduce the manual grading workload and to prioritize the patient grading queues.

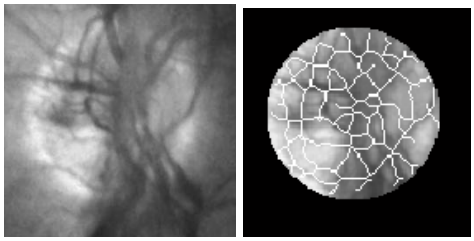

(a) (b)

Fig 3(a) the abnormal disc image. (b)segment classified as abnormal.

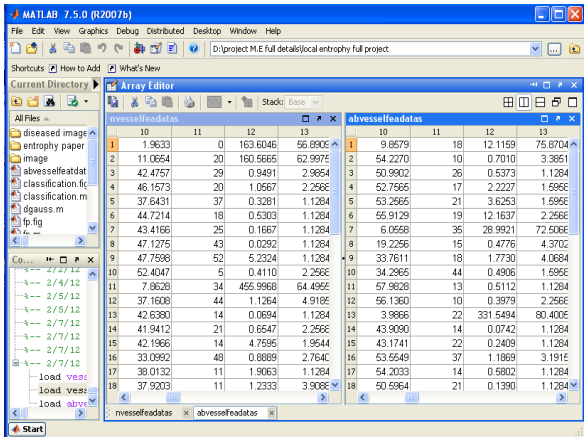

Fig 4 Feature Measurements of Normal and Abnormal blood vessels.

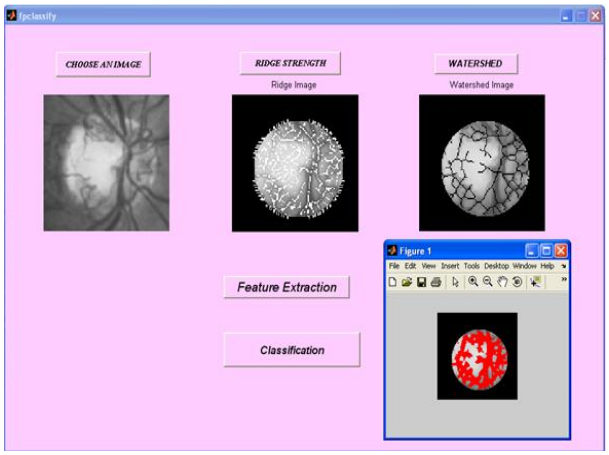

Fig 5 Optic Disc classified as Abnormal

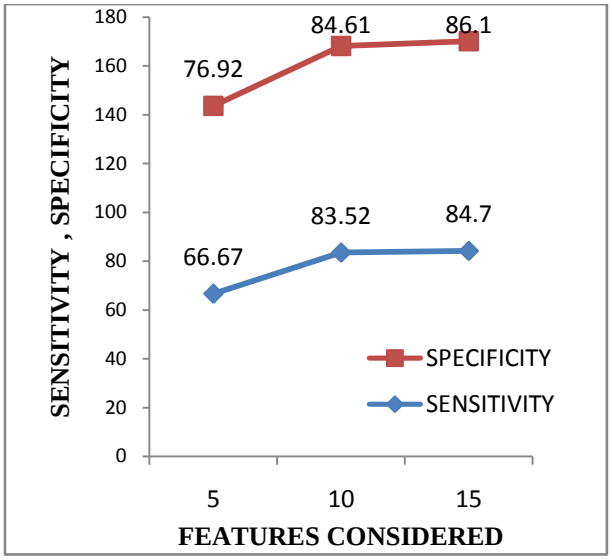

Fig 6 Sensitivity and Specificity

3. CONCLUSION

In this study, a system is developed to detect the new vessels on the optic disc. The new vessels outside the disc are more similar to the new vessels at the disc itself and would be detected by a different detector. However, the combination of this system with the exudates detection system will improve the detection of the proliferative diabetic retinopathy and maculopathy that causes the blindness.

4. REFERENCES

[1] Keith A. Goatman, Alan D. Fleming, Sam Philip, Graeme J. Williams, John A. Olson, and Peter F. Sharp, "Detection of New Vessels on the Optic Disc Using Retinal Photographs,"*IEEE Trans. Med. Imag.*, vol. 30, no. 4,pp.972-979,April 2011.

[2] M. Niemeijer, B. V. Ginneken, J. Staal, M. S. A. Suttorp-Schulten, and M. D. Abramoff, "Automatic detection of red lesions in digital color fundus photographs," *IEEE Trans. Med. Imag.*, vol. 24, no. 5, pp. 584–592, May 2005.

[3] J. H. Hipwell, F. Strachan, J. A. Olson, K. C. McHardy, P. F. Sharp, and J. V. Forrester, "Automated detection of microaneurysms in digital red-free photographs: A diabetic retinopathy screening tool," *Diabetic Med.*, vol. 17, pp. 588–594, 2000.

[4] T. Walter, P. Massin, A. Erginay, R. Ordonez, C. Jeulin, and J. C. Klein, "Automatic detection of microaneurysms in color fundus images," *Med. Image Anal.*, vol. 11, pp. 555–566, 2007.

[5] A. D. Fleming, S. Philip, K. A. Goatman, J. A. Olson, and P. F. Sharp,"Automated detection of exudates for diabetic retinopathy screening," *Phys. Med. Biol.*, vol. 52, pp. 7385–7396, 2007.

[6] C. I. Sánchez, M. García, A. Mayo, M. I. López, and R. Hornero, "Retinal image analysis based on mixture models to detect hard exudates," *Med. Image Anal.*, vol. 13, pp. 650–658, 2009.

[7] M. Niemeijer, B. V. Ginneken, S. R. Russel, M. S. A. Suttorp-Schulten, and M. D. Abramoff, "Automated detection and differentiation of drusen, exudates and cotton-wool spots in digital color fundus photographs for diabetic retinopathy diagnosis," *Investigate Ophthalmol. Vis.Sci.*, vol. 48, pp. 2260–2267, 2007.

[8] C. I. Sánchez, M. García, A. Mayo, M. I. López, and R. Hornero, "Retinal image analysis based on mixture models to detect hard exudates," *Med. Image Anal.*, vol. 13, pp. 650–658, 2009.

[9] A. D. Fleming, K. A. Goatman, S. Philip, G. J.Williams, G. J. Prescott, G. S. Scotland, P. McNamee, G. P. Leese, W. Wykes, P. F. Sharp, and J. A. Olson, "The role of haemorrhage and exudate detection in automated grading of diabetic retinopathy," *Br. J. Ophthalmol.*, vol. 94, no. 6, pp. 706–711, 2010.

[10] T. Walter, J. C. Klein, P. Massin, and A. Erginay, "A contribution of image processing to the diagnosis of diabetic retinopathy-detection of exudates in color fundus images of the human retina," *IEEE Trans. Med. Imag.*, vol. 21, no. 10, pp. 1236–1243, Oct. 2002.

[11] P. H. Gregson, Z. Shen, R. C. Scott, and V. Kozousek, "Automated grading of venous beading," *Comput. Biomed. Res.*, vol. 28, pp. 291–304, 1995.

[12] C. W. Yang, D. J. Ma, S. C. Chao, C. M. Wang, C. H. Wen, C. S. Lo,P. C. Chung, and C. I. Chang, "Computer-aided diagnostic detection system of venous beading in retinal images," *Opt. Eng.*, vol. 39, pp. 1293–1303, 1995.

[13] H. F. Jelinek, M. J. Cree,J. J. G. Leandro, J. V. B. Soares, R. M. C. Jr, and A. Luckie, "Automated segmentation of retinal blood vessels and identification of proliferative diabetic retinopathy," *J. Opt. Soc. Am. A*, vol. 24, pp. 1448–1456, 2007.

[14] A. D. Fleming, S. Philip, K. A. Goatman, J. A. Olson, and P. F. Sharp, "Automatic detection of retinal anatomy to assist diabetic retinopathy screening," *Phys. Med. Biol.*, vol. 52, pp. 331–345, 2007.

[15] Thitiporn Chanwimaluang, Guoliang Fan, and Stephen R. Fransen" Hybrid Retinal Image Registration*" IEEE Trans. on Info.Tech. in Biomedicine* vol. 10, no. 1, pp.129-142, Jan. 2006.

[16] M. Niemeijer, M. D. Abràmoff, and B. van Ginneken, "Fast detection of the optic disc and fovea in color fundus photographs," *Med. Image Anal.*, vol. 13, pp. 869–870, 2009.

[17] Gopal Datt Joshi, Jayanthi Sivaswamy and S. R. Krishnadas,"Optic Disk and Cup Segmentation From Monocular Color Retinal Images for Glaucoma Assessment", *IEEE Trans. Med. Imag.*, vol. 30, no. 6, pp. 1192–1205, Mar. 2011.

[18] A. Hoover, V. Kouznetsova, and M. Goldbaum, "Locating blood vessels in retinal images by piecewise threshold probing of a matched filter response," *IEEE Trans. Med. Imag.*, vol. 19, no. 3, pp. 203–210, Mar. 2000.

[19] F. Zana and J. C. Klein, "Segmentation of vessel-like patterns using mathematical morphology and curvature evaluation," *IEEE Trans. Image Process.*, vol. 10, no. 7, pp. 1010–1019, Jul. 2001.

[20] J. J. Staal, M. D. Abr'amoff, M. Niemeijer, M. A. Viergever, and B. V. Ginneken, "Ridge based vessel segmentation in color images of the retina," *IEEE Trans. Med. Imag.*, vol. 23, no. 4, pp. 501–509, Apr. 2004.

[21] T. Lindeberg, "Scale-space theory:A basic tool for analysing structures at different scales," *J. Appl. Stat.*, vol. 21, pp. 225–270, 1994.

[22] F. Meyer, "Topographic distance and watershed lines," *Signal Process.*, vol. 38, pp. 113–125, 1994.

[23] T. Walter and J. C. Klein, "Ch. Automatic Analysis of Color Fundus Photographs and its Application to the Diagnosis of Diabetic Retinopathy," in *Handbook of Biomedical Image Analysis*. New York: Kluwer Academic/Plenum, 2005, vol. II, Segmentation Models, pt. B, pp. 315–368.

[24] Keith A. Goatman, Alan D. Fleming, Sam Philip,Graeme J. Williams, John A. Olson, and Peter F. Sharp "Detection of New Vessels on the Optic Disc Using Retinal Photographs" *IEEE Trans. Med. Imag.*, vol. 30, no. 4, pp. 972–979, Apr. 2011.

[25] B. E. Boser, I. Guyon, and V. Vapnik, "A training algorithm for optimal margin classifiers," in *Proc. 5th Annu. Workshop Computat. Learn. Theory*, 1992, pp. 144–152.

[26] V. N. Vapnik, *Statistical Learning Theory*. New York: Wiley, 1998.

[27] T. F. Wu, C. J. Lin, and R. C. Weng, "Probability estimates for multiclass classification by pairwise coupling," *J. Mach. Learn. Res.*, vol. 5, pp. 975–1005, 2004.